Activity Level of an Atrial Ectopic Focus Observed through the Atrial Vectorcardiogram: A Biophysical Model

M Lemay[1], V Jacquemet[1], C Duchêne[1], A van Oosterom[3],
R Abächerli[2], JM Vesin[1]

[1]Ecole polytechnique Fédérale de Lausanne, Lausanne, Vaud, Switzerland
[2]Schiller AG, Baar, Zug, Switzerland
[3]Centre Hospitalier Universitaire Vaudois, Lausanne, Vaud, Switzerland

Abstract

This study aims at assessing the relation between the activity level of an ectopic focus and the complexity of the resulting atrial fibrillation (AF) dynamics. Eight different episodes of focal AF were simulated in a 3D model of human atria. To create various AF dynamics, the episodes differed by the location of their focal source. The activity level of a source was quantified by the number of propagating focal fronts originating from that source. The dynamic complexity was quantified through the time course of the atrial vectorcardiogram (VCG) orientation. The eigenvalues of the second-order raw moment matrix of the normalized atrial VCG were used to characterize the spread of spatial distribution of the atrial VCG. A strong correlation was found between the 3rd eigenvalues and the number of focal fronts. Analyzing the spatial distribution of the atrial VCG could provide information about the activity level of atrial ectopic foci and the complexity of AF dynamics.

1. Introduction

The onset and maintenance of atrial fibrillation (AF) require both an initiating event and an arrhythmogenic substrate. Possible mechanisms of AF include multiple reentrant wavelets [1] or "focal" mechanisms with fibrillatory conductions [2]. The hypothesis of focal mechanism refers to the observation of atrial myocytes spontaneously firing at a high rate (> 240 beats per minute), also named ectopic foci. Atrial myocytes characterized by automatic electrical activity have been mainly observed in the pulmonary vein (PV) region. That explains the relative success of the standard ablation procedure consisting in the electrical isolation of all PVs without actual localization of the focal trigger [3]. However, firing sites have been observed outside the targeted ablation area in the PVs [4]. These non-PV firing sites may complicate the ablation procedure or be responsible for its lack of success. This has

encouraged the search for signal processing tools to estimate (before the ablation procedure) the localization of these focal firing sites. Different localization approaches have been proposed [5–7]. Duchêne et al. [7] proposed using the atrial vectorcardiogram (VCG) to identify stable AF sources with different rates evolving simultaneously. In this simulation study, the time course of the electrical dipole generated by each of the reentrant circuit was successfully reconstructed from non-invasive recordings.

This paper addresses the question of whether it is possible to determine the impact of a focal source, presumed unique, on the AF dynamics based on ECG recordings. If the source perturbs significantly the AF dynamics, its electrical isolation in an ablation procedure is likely to decrease AF complexity or prolong cycle lengths. If the focal source is "silent", its electrical isolation may be unnecessary. In this study based on simulated AFs involving a single focal source, the number of propagating fronts originating from the source in a fixed time window was used as a descriptor of the impact of the source on the AF dynamics, referred to as the activity level of the focal source. We hypothesized that episodes of focal AF maintained by a source with a high activity level are associated with AF dynamics of lower spatial complexities. To measure spatial complexity, we will use the eigenvalues of the matrix of the second order moments of the normalized atrial VCG [8] as features to discriminate "active" focal sources from "silent" ones.

2. Methods

2.1. Simulated focal AF

A three-dimensional, thick-walled, biophysical model of the atria was developed based on magnetic resonance (MR) images, which simulates the propagation of the electrical impulse [9]. Figure 1A shows the resulting atrial geometry. The major anatomical details are also indi-

cated. The electrical propagation of the cardiac impulse was simulated using a reaction-diffusion system (monodomain formulation) based on a detailed ionic model of the cell membrane kinetics, the Courtemanche *et al.* model [10], comprising a total of 800,000 units. In order to create a substrate for AF, patchy heterogeneities in action potential duration were introduced by modifying the local membrane properties [11].
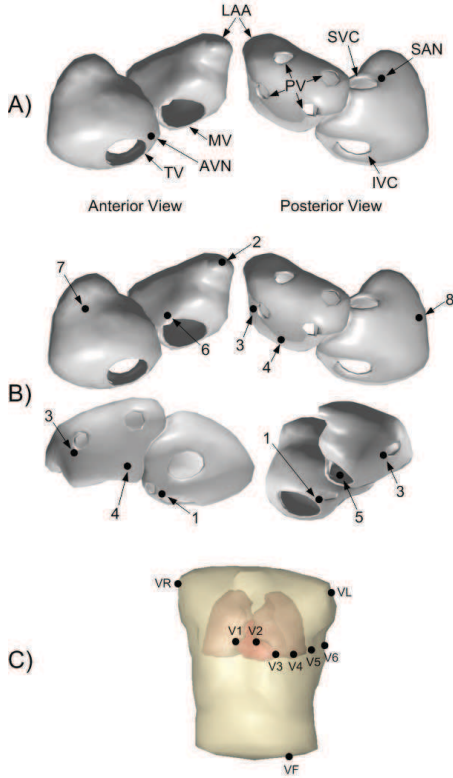
Figure 1. A) Geometry of the atrial model as seen from an anterior view (left) and a posterior view (right). The major anatomical details shown, including those blocking propagation: the tricuspid valve (TV), the mitral valve (MV), the inferior vena cava (IVC), the superior vena cava (SVC), and the four pulmonary veins (PVs). The location of the sinoatrial node (SAN), the atrioventricular node (AVN) and the left atrium appendage (LAA) are indicated. B) The locations of the eight simulated focal sources as seen from an anterior view (upper left), a posterior view (upper right), an inferior view (lower left) and a nearly left view (lower right). C) Geometry of the compartmental torso model (nearly frontal view) including the atria, the ventricles, the lungs, and the position of the nine electrodes of the standard 12-lead system.

Eight different clinical sites were selected in the left and right atrium. These locations are shown in Figure 1B. They correspond to typical locations of focal sources reported in the clinical literature. For each of these sites, a 10-second episode of focal AF was simulated. Sources were modeled by spontaneous activations at a fixed cycle length. The cycle length of these sources (mean±standard deviation: 168±0.12 ms; range: 158 and 195 ms) was adjusted to the local effective refractory period in order to initiate AF. The activity level of these sources was quantified by the number of propagating focal fronts n_f originating from the firing sites over their entire 10-second simulation. These propagating focal fronts were identified by visual inspection of the membrane potential maps. Figure 2 shows two typical cases of focal fronts originating from the source that precede another wavefront by a long (A) and a short (B) intervals, and a typical case (C) where source firing does not produce a focal front due to the passage of the wavefront.

Body surface potential maps $\mathbf{\Phi}_{ECG}$ of atrial activities were computed at 670 points. The source description used was the equivalent double layer specified at the closed surface bounding the myocardium [11]. The local double layer strength at the surface was taken to be the time course of the transmembrane potential computed in the atrial model. The effect of volume conduction heterogeneity on the atrial contribution to body surface potentials was computed by means of the boundary element method. This was applied to a compartmental torso model, including the ventricles, blood cavities and the lungs [11]. Figure 1C displays this torso geometry, also derived from MR images.

2.2. Estimated atrial equivalent dipole

The time course of the atrial VCG $\mathbf{V}(t)$ which constitutes an estimate of the atrial equivalent dipole was computed for each of the eight AF simulations. These atrial VCGs were derived from a linear combination of the 670 ECG signals as follows [12]:

$$\mathbf{V}(t) = [V_x(t)\ V_y(t)\ V_z(t)]^T = \mathbf{T}\mathbf{\Phi}_{ECG}(t), \quad (1)$$

with $\mathbf{T}$ being a matrix of size 3×670 that produces the estimated the x-, y-, and z-components $(V_x(t), V_y(t), V_z(t))$ of the atrial VCG from the body surface potential map $\mathbf{\Phi}_{ECG}(t)$ at each time index t. The symbol $[]^T$ denotes the transposition operator.

2.3. Spatial distribution features

For each atrial VCG $\mathbf{V}(t)$, a 3×3 matrix $\mathbf{C}$ comprizing the second-order moments of the normalized signals was computed over the time interval $[t_1, t_2]$ as:

$$\mathbf{C} = \frac{1}{t_2 - t_1} \int_{t_1}^{t_2} dt\ \frac{\mathbf{V}(t) \cdot \mathbf{V}(t)^\top}{\|\mathbf{V}(t)\|^2}, \quad (2)$$

where $\|(\cdot)\|$ stands for the norm of $(\cdot)$. The eigenvalues of $\mathbf{C}$, λ_1, λ_2, and λ_3 in descending order were taken as

measures of spatial complexity as suggested in [13]. The matrix $\mathbf{C}$ was computed over the entire 10-second interval.

3. Results

Different types of AF dynamics were observed in the eight simulated episodes, from broad wavelets/stable macroreentries to multiple wavelets/spirals. Table 1 displays, for each of the eight simulations, the location of its source (Figure 1B), the number of effective focal fronts nf over the number of source firings, and the 1st, 2nd and 3rd eigenvalues λ_1, λ_2, and λ_3. The number of focal fronts ranged from 21 to 43 (30.9 ± 7.2) within the 10-second interval. The 1st, 2nd and 3rd eigenvalues varied between

0.42 and 0.62, 0.21 and 0.37, and 0.13 and 0.23, respectively (0.50 ± 0.08, 0.31 ± 0.06, 0.19 ± 0.03, respectively). The maximum of the dipole spatial distribution consistently pointed toward the location of the source when the dynamic complexity was low (high value of λ_1). The highest correlation (-0.93) was found between the 3rd eigenvalues and the numbers of focal fronts nf, see Figure 3. As for the 1st and 2nd eigenvalues, the correlation values were 0.78 and -0.52, respectively.

Table 1. Information on the eight AF simulations including the location of their single firing site, their number of focal fronts over the number of source firings within 10 seconds, and the 1st, 2nd and 3rd eigenvalues of the atrial VCG matrix $\mathbf{C}$.

Focal trigger	Focal fronts	λ_1	λ_2	λ_3
Site n° 1	30 / 63	0.43	0.37	0.20
Site n° 2	43 / 63	0.62	0.22	0.16
Site n° 3	34 / 51	0.52	0.28	0.20
Site n° 4	24 / 58	0.43	0.36	0.21
Site n° 5	29 / 58	0.45	0.33	0.22
Site n° 6	21 / 62	0.46	0.31	0.23
Site n° 7	38 / 61	0.47	0.36	0.17
Site n° 8	28 / 60	0.60	0.27	0.13
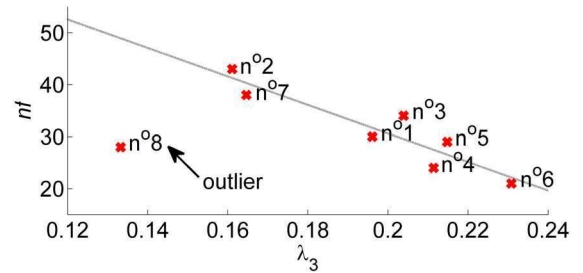
Figure 3. Scattergram of the number of propagating fronts nf originating from one of the eight focal firing sites as a function of the spatial complexity of the atrial VCG (λ_3). The gray line represents the linear fit in the least-square sense, excluding the outlier.

4. Discussion and conclusions

Interestingly, it was observed that changes in the location of focal sources, without any substrate modifications, may produce different AF dynamics. Our simulations suggest that analyzing the spatial distribution of the atrial VCG estimated from the entire body surface potential map may provide information about the activity level of atrial ectopic foci. As mentioned in [8], the third eigenvalue λ_3 characterizes the spread of spatial distribution of

Figure 2. A) Typical example (simulation 5, see Table **??**) of a focal front originating from the source that precedes another wavefront by a long time interval. B) Typical example (simulation 5) of a focal front originating from the source that precedes another wavefront by a short time interval. C) Typical example (simulation 5) of a source burst pacing during a wavefront passage. In this case, we take it that the front does not originate from the source. The source location is identified by circles and the wavefront directions on the left atrium are indicated by arrows.

the atrial VCG. A large λ_3 is associated with a complex AF dynamic. The first and second eigenvalues λ_1 and λ_2 characterize a modal or bimodal spatial distribution and a spatial distribution over a great circle, respectively. Large λ_1 and λ_2 values are associated with focal atrial activities and macro-reentrant circuits/broad wavelets, respectively. It explains why the first eigenvalues λ_1 are correlated with the activity level of the focal sources (0.78). However, the third eigenvalues λ_3 produced a higher correlation magnitude (-0.93). The third eigenvalues λ_3 discriminate complex AF dynamics from focal, macro-reentry, and broad wavelet dynamics. Therefore, the simulated AFs characterized by ectopic foci producing wave fronts in a preferential direction are closer to a broad wavelet mechanisms than to the typical focal ones.

The fact that our approach does not differentiate active focal sources from stable reentrant circuits constitutes its principal limitation. This is illustrated by the outlier shown in Figure 3, which was characterized by the lowest dynamic complexity (a 3rd eigenvalue of 0.13) in spite of a non-extreme number of focal fronts (28) caused by a stable macro-reentry masking the focal source. The combination of the three eigenvalues may be helpful in attempts to quantify the activity level of the source and its type of mechanism (focal or reentrant circuits).

Based on our simulations, the analysis of the spatial complexity of the atrial VCG may constitutes a promising approach for predicting non-invasively (before the intervention) the effort (and, thereby, the time) needed to isolate all AF sources by catheter ablation.

Acknowledgements

References

[1] Allessie MA, Konings K, Kirchhof C, Wijffels M. Electrophysiologic mechanisms of perpetuation of atrial fibrillation. Am J Cardiol 1996;77(3):10A–23A.

[2] Haissaguerre M, Jais P, Shah DC, Takahashi A, Hocini M, Quiniou G, Garrigue S, Le Mouroux A, Le Metayer P, Clementy J. Spontaneous initiation of atrial fibrillation by ectopic beats originating in the pulmonary veins. N Eng J Med 1998;339:659–666.

[3] Haissaguerre M, Jais P, Shah DC, Garrigue S, Takahashi A, Lavergne T, Hocini M, T PJ. Electrophysiologic end point for catheter ablation of atrial fibrillation initiated from multiple pulmonary venous foci. Circulation 2000;101:1409–1417.

[4] Lin JL, Lai LP, Tseng YZ, Lien WP, Huang SKS. Global distribution of atrial ectopic foci triggering recurrence of atrial tachyarrhythmia after electrical cardioversion of long-standing atrial fibrillation: a bi-atrial basket mapping study. J Am Coll Cardiol 2001;37:904–910.

[5] Sippens Groenewegen A, Natale A, Marrouche NF, Bash D, Cheng J. Potential role of body surface ECG mapping for localization of atrial fibrillation trigger sites. J Electrocardiol 2004;37:47–52.

[6] van Dam P, Oostendorp TF, van Oosterom A. Application of the fastest route algorithm in the interactive simulation of the effect of local ischemia on the ECG. Med Biol Eng 2009;47(1):11–20.

[7] Duchêne C, Lemay M, Vesin JM, van Oosterom A. Estimation of atrial multiple reentry circuits from surface ECG signals based on a vectorcardiogram approach. In Proc. Functional Imaging and Modeling of the Heart 2009, volume 5528. 2009; 277–284.

[8] Lemay M, Vesin JM, van Oosterom A, Jacquemet V, Kappenberger L. Spatial dynamics of atrial activity assessed by the vectorcardiogram: from sinus rhythm to atrial fibrillation. Europace 2007;9:vi109–vi118.

[9] Jacquemet V, Virag N, Ihara Z, Dang L, Blanc O, Zozor S, Vesin JM, Kappenberger L, Henriquez CS. Study of unipolar electrogram morphology in a computer model of atrial fibrillation. J Cardiovasc Electrophysiol 2003; 14(10(Suppl.)):S172–S179.

[10] Courtemanche M, Ramirez RJ, Nattel S. Ionic mechanisms underlying human atrial action potential properties: Insights from a mathematical model. Am J Physiol 1998; 275:H301–H321.

[11] van Oosterom A, Jacquemet V. Genesis of the P wave: atrial signals as generated by the equivalent double layer source model. Europace 2005;7 (suppl. 2):S21–S29.

[12] van Oosterom A, Ihara Z, Jacquemet V, Hoekema R. Vectorcardiographic lead systems for the characterization of atrial fibrillation. J Electrocardiol 2007;40(4).

[13] Jacquemet V, Lemay M, van Oosterom A, Kappenberger L. The equivalent dipole used to characterize atrial fibrillation. In Computers in Cardiology 2006, volume 33. 2006; 149–152.

Address for correspondence:

Mathieu Lemay
Department of Physiology
University of Bern
CH-3012 Bern
Switzerland
mathieu.lemay@epfl.ch